



OPEN

Clinical feasibility of deep learning-driven magnetic resonance angiography collateral map in acute anterior circulation ischemic stroke

Ye Jin Jeon^{1,10}, Hong Gee Roh^{2,3,10}, Sumin Jung⁴, Hyun Yang⁴, Hee Jong Ki⁵, Jeong Jin Park⁶, Taek-Jun Lee⁷, Na Il Shin⁵, Ji Sung Lee⁸, Jin Tae Kwak^{3,4} & Hyun Jeong Kim^{3,8,9}✉

To validate the clinical feasibility of deep learning-driven magnetic resonance angiography (DL-driven MRA) collateral map in acute ischemic stroke. We employed a 3D multitask regression and ordinal regression deep neural network, called as 3D-MROD-Net, to generate DL-driven MRA collateral maps. Two raters graded the collateral perfusion scores of both conventional and DL-driven MRA collateral maps and measured the grading time. They also qualitatively assessed the image quality of both collateral maps. Interrater and inter-method agreements for collateral perfusion grading between the two collateral maps were analyzed, along with a comparison of grading time and image quality. In the analysis of the 296 acute ischemic stroke patients, the inter-method agreement for collateral perfusion grading was almost perfect ($\kappa = 0.96$, 95% CI: 0.95–0.98). Compared to conventional MRA collateral maps, the time taken for collateral perfusion grading on DL-driven MRA collateral maps was shorter ($P < 0.001$ for rater 1 and $P = 0.003$ for rater 2), and the image quality of the DL-driven MRA collateral maps was superior ($P < 0.001$ for rater 1 and $P = 0.002$ for rater 2). The DL-driven MRA collateral map demonstrates clinical feasibility for collateral perfusion grading in acute ischemic stroke, with the added benefits of reduced generation and interpretation time, along with improved image quality of the MRA collateral map.

Keywords Cerebrovascular disorders, Stroke, Collateral circulation, Deep learning, Magnetic resonance imaging, Artificial intelligence

Abbreviations

3D-MROD-Net	3-dimensional multitask regression and ordinal regression deep neural network
CI	Confidence interval
CPS	Collateral perfusion score
CT	Computed tomography
D	Dimensional
DASAN	Database of acute ischemic stroke analysis network

¹Department of Computer Science, University of California, La Jolla, San Diego, CA, USA. ²Department of Radiology, Konkuk University Medical Center, Konkuk University School of Medicine, Seoul, Republic of Korea. ³DeepClue Inc., Daejeon, Republic of Korea. ⁴School of Electrical Engineering, Korea University, 145 Anam-ro, Seongbuk-gu, 02841 Seoul, Republic of Korea. ⁵Department of Neurosurgery, Daejeon St. Mary's Hospital, College of Medicine, The Catholic University of Korea, Daejeon, Republic of Korea. ⁶Department of Neurology, Konkuk University Medical Center, Konkuk University School of Medicine, Seoul, Republic of Korea. ⁷Department of Neurology, Daejeon St. Mary's Hospital, College of Medicine, The Catholic University of Korea, Daejeon, Republic of Korea. ⁸Clinical Research Center, Asan Institute for Life Science, Asan Medical Center, University of Ulsan College of Medicine, Seoul, Republic of Korea. ⁹Department of Radiology, Daejeon St. Mary's Hospital, College of Medicine, The Catholic University of Korea, 64 Daeheung-Ro, Jung-Gu, 34943 Daejeon, Republic of Korea. ¹⁰Ye Jin Jeon and Hong Gee Roh equally contributing as co-first authors. ✉email: jkwak@korea.ac.kr; mskendy429@gmail.com

DCE-MRA	Dynamic contrast-enhanced magnetic resonance angiography
DWI	Diffusion-weighted imaging
MCA	Middle cerebral artery
MRI	Magnetic resonance imaging
MRP	Magnetic resonance perfusion

Cerebral collateral circulation maintains perfusion to the ischemic brain despite arterial occlusion, using alternative vascular channels. In cerebral ischemia due to proximal arterial steno-occlusion, tissue and functional outcomes mainly depend on the collateral circulation, which has high interindividual variability^{1,2}. Previous studies have demonstrated that good collateral circulation slow infarct progression, while poor collateral circulation expedites it, correlating with larger infarct growth and poorer functional outcomes, even with timely recanalization^{3–7}. Thus, accurate collateral status assessment is crucial for treatment decisions in acute ischemic stroke patients.

Recently, a multiphase collateral imaging method, derived from dynamic susceptibility contrast-enhanced magnetic resonance perfusion or dynamic contrast-enhanced magnetic resonance angiography (DCE-MRA), known as the magnetic resonance perfusion (MRP) collateral map and MRA collateral map, respectively, has been developed⁸. The MRP and MRA collateral maps consist of five-phase images tailored to the individual patient's hemodynamics, including arterial, capillary, early venous, late venous, and delay phases, which provide brain parenchymal perfusion status, as well as collateral vessels. Clinical studies of the MRA collateral map have demonstrated the predictability of functional and tissue outcomes^{9,10}, suggesting the feasibility of a 3-minute MR imaging (MRI) protocol that includes diffusion-weighted imaging (DWI) and DCE-MRA. This protocol provides precise information on baseline lesion, causative vessel, penumbra, and collateral perfusion status, all of which are essential for treatment decisions.

Deep learning (DL) techniques have contributed to overcoming the limitations of classical techniques in the generation and interpretation of medical images by eliminating manual operation and heuristic decisions or estimations made by medical experts^{11–14}. By applying DL to generate collateral maps, the process can be automated, allowing for prompt treatment even in settings with limited medical infrastructure. A few research endeavors rooted in deep learning have aimed to autonomously generate an MRP collateral map. For instance, a 3-dimensional (D) deep regression neural network was developed to derive the MRP collateral map¹⁵. Additionally, a 3D multitask regression and ordinal regression deep neural network (3D-MROD-Net) was proposed to further enhance the quality of the MRP collateral map by integrating ordinal regression and atrous spatial pyramid pooling¹⁶, which is the state-of-the-art collateral map generation method (Fig. 1). However, DL techniques have not been applied to the generation of MRA collateral maps. When using an MRP collateral map to evaluate patients with acute ischemic stroke, additional vascular imaging is required to identify occluded vessels. However, with an MRA collateral map, no additional vascular imaging is necessary, thereby minimizing the imaging protocol and acquisition time in this time-sensitive disease. Herein, we aimed to generate an DL-driven MRA collateral map using 3D-MROD-Net and validate its clinical feasibility in acute ischemic stroke by comparing it with conventional MRA collateral map.

Materials and methods

The local institutional review boards of Konkuk University Medical Center (KUMC0114-01-100-007) and Daejeon St. Mary's Hospital (DC16OIMI0043) approved this study, and written informed consent was obtained from all patients. All methods were carried out in accordance with relevant guidelines and regulations of the Declaration of Helsinki and the Strengthening the Reporting of Observational Studies in Epidemiology (STROBE) guidelines for reporting observational study. Two hundred fourteen patients who were included in this study have been previously reported. The prior articles addressed the prognostic value, predictability of hemorrhagic transformation, infarct growth, and futile recanalization, and penumbral accessibility in acute ischemic stroke, as well as the use of deep learning methods for generating the MRP collateral map^{7–10,15–19}. In contrast, this study focused on the application of deep learning method for generating the MRA collateral map.

Patients cohort for collateral map

For this retrospective analysis, we selected patients from the ongoing Database of Acute ischemic Stroke Analysis Network (DASAN), which includes imaging and clinical data of patients with acute ischemic stroke resulting from large vessel occlusion (Fig. 2). These data were prospectively collected from two university hospitals from January 1, 2016. The inclusion criteria for DASAN patients were as follows: (1) were older than 18 years of age; (2) had acute ischemic stroke due to occlusion or severe stenosis of the internal carotid artery and/or M1 or M2 segment of the middle cerebral artery (MCA) or the basilar artery; and (3) had undergone brain computed tomography (CT) and MRI, including DWI (Figs. 3A, 4A, 5A), susceptibility-weighted imaging, DCE-MRA, dynamic susceptibility contrast-enhanced MRP, and fluid attenuated inversion recovery at admission.

Patients cohort for training 3D-MROD-Net to generate the DL-driven MRA collateral map

To train 3D-MROD-Net for generating the DL-driven MRA collateral map, we selected 964 consecutive patients, collected from January 1, 2016, to December 31, 2019, from DASAN. Of these patients, 719 patients had acute infarct lesions due to arterial steno-occlusive lesions (663 patients in anterior circulation territories and 56 patients in posterior circulation territories) on DWI at admission. The remaining 245 patients were identified as having neither acute infarct lesions nor arterial steno-occlusive lesions. A total of 908 patients with acute infarct lesions in the anterior circulation territory (ischemic patients) and without acute infarct lesions (nonischemic controls) were divided into a training set, a validation set, and a test set in chronological order with a ratio of 0.5:0.2:0.3 (Fig. 2). The training set, validation set, and test set included 453 subjects (395 patients

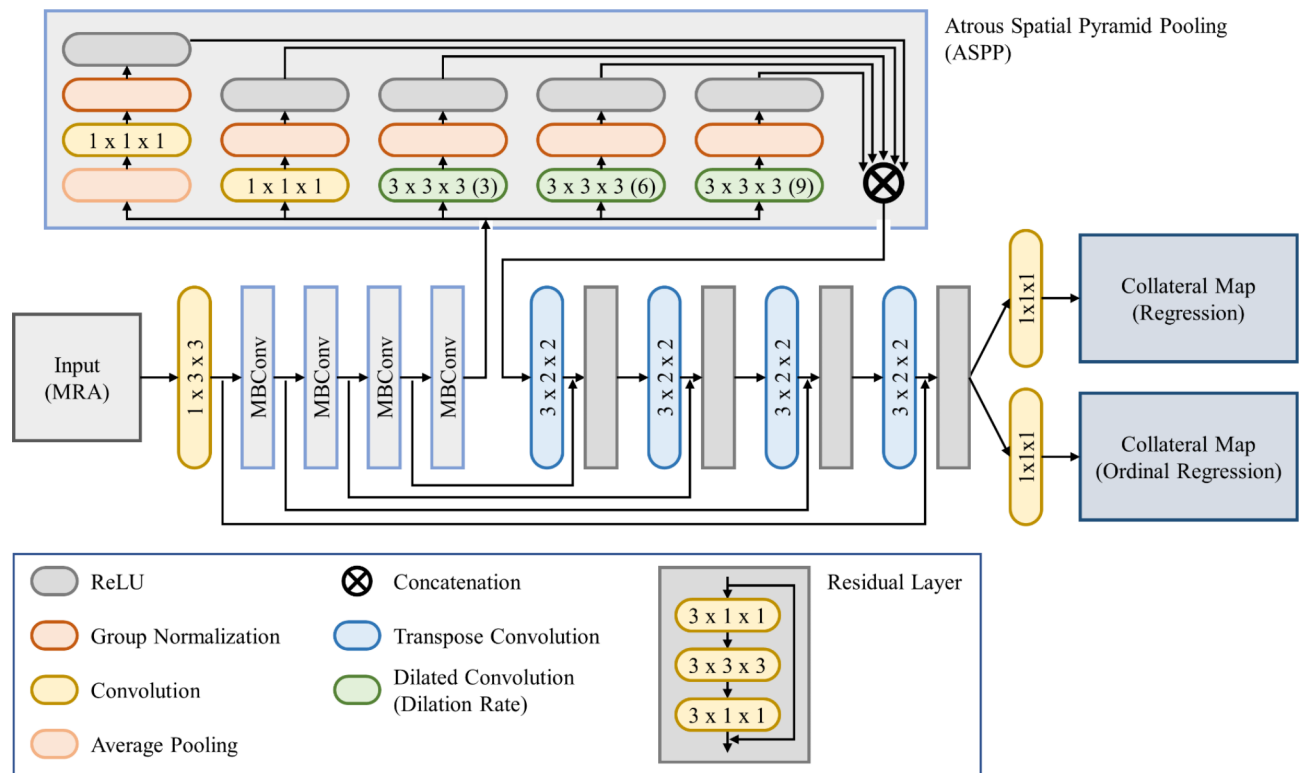


Fig. 1. Architecture of 3D-MROD-Net. 3D-MROD-Net is built based upon an encoder-decoder architecture. The encoder uses a convolution layer and a series of mobile inverted bottleneck convolution blocks (MBCConv). The decoder involves a set of transpose convolution layer and a residual layer. The output of the decoder is used to generate two types of collateral maps. The first type is the collateral maps in a continuous range. The second type is the collateral maps in an ordinal order. The second type is used during training only to enhance the training efficiency.

and 58 controls), 181 subjects (137 patients and 44 controls), and 274 subjects (145 patients and 129 controls), respectively.

Patients cohort for clinical validation of the DL-driven MRA collateral map

For the evaluation of the DL-driven MRA collateral map, a total of 335 patients were selected from the DASAN between January 1, 2020, and March 31, 2023. These patients do not overlap with the dataset used for training 3D-MROD-Net (Fig. 2). Among them, 296 patients with acute ischemic stroke due to occlusion or severe stenosis of the ICA and/or M1 or M2 segment of the MCA were included, following the exclusion of 39 patients with acute ischemic stroke due to occlusion or severe stenosis of the basilar artery. The patients were evaluated based on demographic data, medical history, vascular risk factors, routine blood tests, brain imaging, and cardiological tests. The severity of stroke was assessed with the National Institutes of Health Stroke Scale (NIHSS).

Imaging protocol and postprocessing for generation of MRA collateral maps

MRI was performed with 3-Tesla MRI scanners (Skyra, Siemens Healthcare, Erlangen, Germany for 963 patients and Ingenia, Philips Healthcare, Best, Netherlands for 241 patients). The acquisition parameters were the same as those used in a previous study⁸. A low-dose protocol was implemented for DCE-MRA²⁰ with acquisition parameters of 2.62/0.95 TR/TE (ms), 90° flip angle, 1446 bandwidth, 5/2 slice thickness/gap (mm), 240 × 240 FOV (mm), 128 × 128 matrix size (mm), 60 measurements, and a temporal resolution of 1.6 s per dynamic acquisition. Using raw data from DCE MRA, 3D arteriography was conducted to assess arterial status (Figs. 3B, 4B, 5B), and an MRA collateral map was reconstructed for collateral perfusion evaluation (C-G of Figs. 3, 4, 5). We generated a conventional MRA collateral map by using an in-house program. The utilized methodology was the same as that used in previous studies⁸. The postprocessing time that was required to generate the conventional MRA collateral map was approximately 5 min.

To generate the DL-driven MRA collateral map (H-L of Figs. 3, 4 and 5), each DCE-MRA dataset underwent the following preprocessing steps. Initially, the raw DCE-MRA data, which were collected as coronal vascular images, were rotated by 90 degrees to generate the DL-driven MRA collateral map in axial brain images. Subsequently, the image slice of the raw DCE-MRA data was adjusted to align with the reconstruction parameters of the conventional MRA collateral map. This adjustment was achieved by interpolating the image slices of the raw DCE-MRA images to match the image slices in the conventional MRA collateral map. The subsequent preprocessing steps were the same as those used in previous studies¹⁶. We utilized 3D-MROD-Net, which was

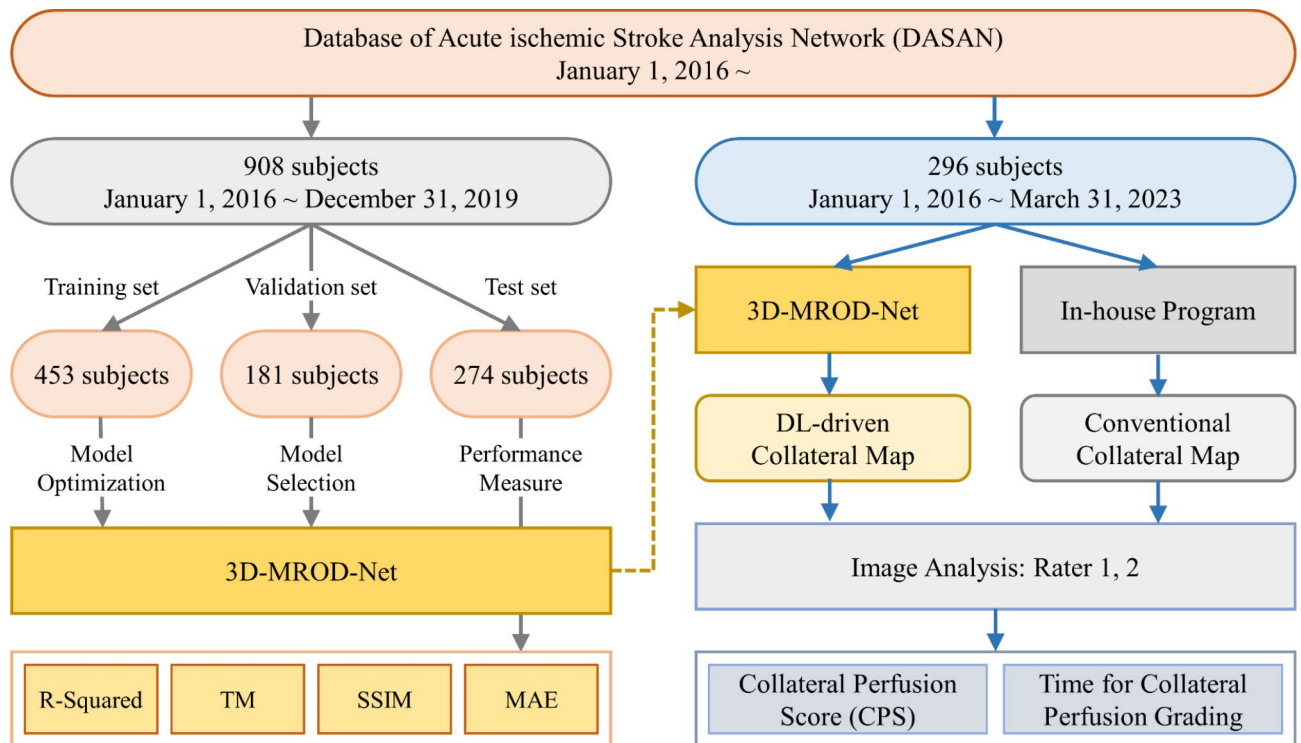


Fig. 2. Flowchart shows subject selection and study methods.

previously published and was designed for generating the MRP collateral map¹⁶, to produce the MRA collateral map. We followed the training, validation, and testing procedures of the previous study¹⁶. 3D-MROD-Net involved an encoder, atrous spatial pyramid pooling (ASPP)¹⁶, and a decoder. The encoder used the architecture of EfficientNetB0 where 2D convolutions are replaced by 3D convolutions. ASPP was used to utilize multi-scale semantic information of feature maps. The decoder contained four sets of decoding layers and residual layers and prediction layers. The decoding layers were used to double the size of the feature maps. The prediction layers had two branches: a regression branch and an ordinal regression branch. The ordinal regression branch, responsible for predicting the ordinal values of collateral maps, was utilized during training only. A horizontal flip was applied as a data augmentation technique due to the left-right symmetry of the brain. The input dimensions of the model were aligned with those of the DCE-MRA data. The required postprocessing time to generate the DL-driven MRA collateral map was approximately 32 s. The R-squared, Tanimoto measure, structural similarity index measure, and mean absolute error values were computed for each of the five phases of the collateral maps per subject within the test set to evaluate the network performance.

Imaging analysis

Baseline DWI lesion volumes were quantified by using MEDIHUB STROKE software (version 2.1.0; JLK Inc., Seoul, Korea)²¹. An experienced (a neuroradiologist with 21 years of experience [rater 1]) and an inexperienced (a fourth-year neurosurgery resident [rater 2]) raters as, who were blinded to all clinical and other imaging data, independently assessed the CP scores (CPSs) of the conventional and DL-driven MRA collateral maps in a blinded fashion on 2 separate occasions at 1 week apart. The CPSs were as follows: 5, excellent; 4, good; 3, intermediate to good; 2, intermediate to poor; 1, poor; and 0, very poor (Table 1)^{9,10}. Two raters determined the final CPSs via consensus. Two raters measured the time taken for collateral perfusion grading and qualitatively evaluated the image quality of the collateral maps by assigning a score of 0 for areas where determination of the CPS was difficult within the following 8 regions of the MCA territory (the insula, subcortical structures [basal ganglia and internal capsule], and M1-M6 regions of the Alberta Stroke Programme Early CT Scores)^{8,22} and a score of 1 for areas where there was no difficulty.

Statistical analysis

Patient characteristics are expressed as the mean (standard deviation [SD]), median (interquartile range [IQR]) or number of participants (%). Differences in the distribution of patient characteristics among collateral perfusion grades were identified by using the chi-square test, Fisher's exact test, ANOVA and the Kruskal-Wallis test, as appropriate. The interrater reliabilities for collateral perfusion grading of both collateral maps and the inter-method agreement between the conventional and DL-driven MRA collateral maps were measured via the Cohen's weighted kappa (κ) with 95% confidence interval (CI). κ was interpreted by the criteria of Landis and Koch as follows: < 0, less than chance agreement; 0.01–0.20, slight agreement; 0.21–0.40, fair agreement; 0.41–0.60, moderate agreement; 0.61–0.80, substantial agreement; and 0.81–1.00, almost perfect agreement²³.

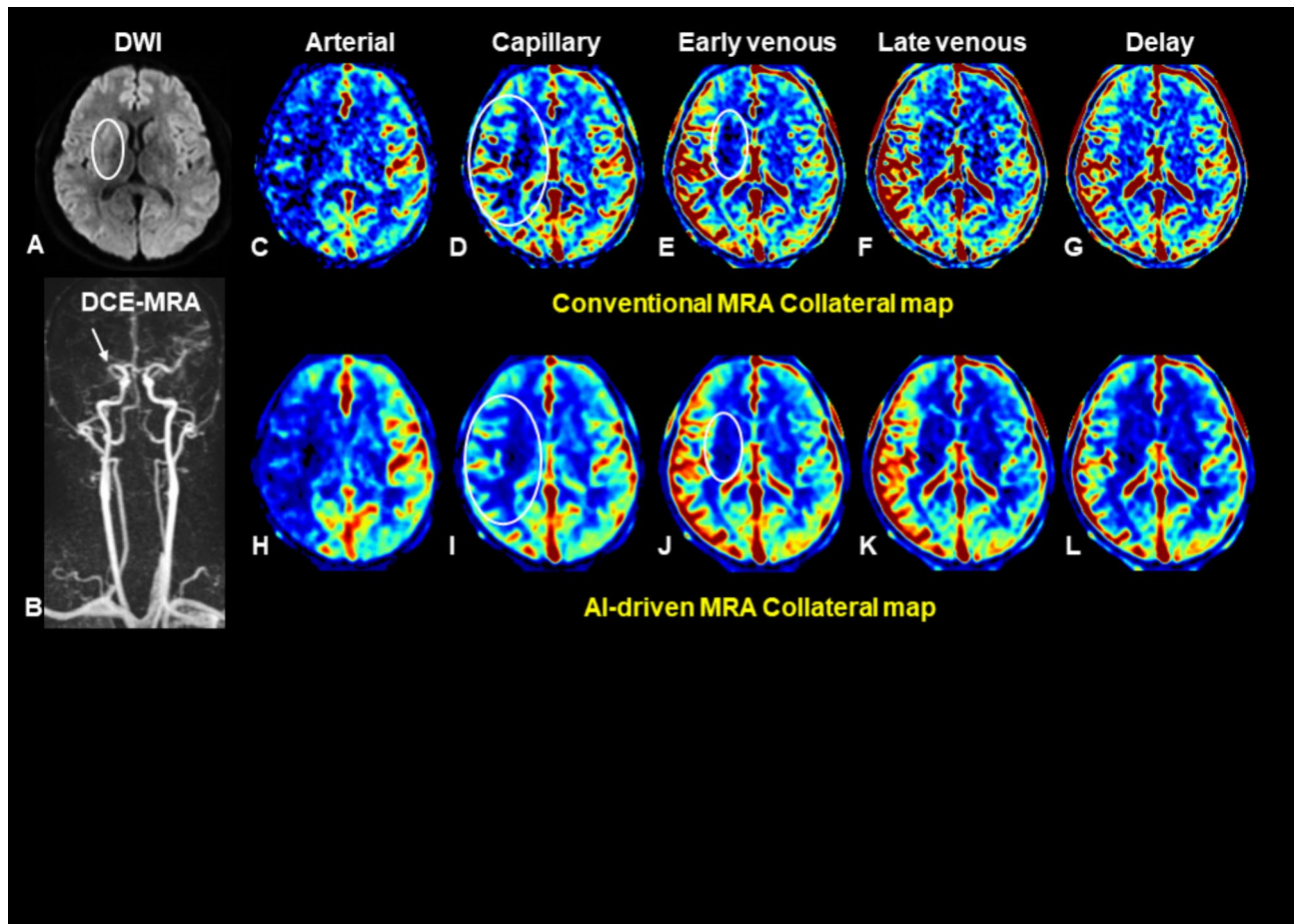


Fig. 3. Images of a middle-aged patient at admission. The diffusion-weighted image (DWI) (A) shows an acute infarction in the right middle cerebral artery (MCA) territory (circle). Dynamic contrast-enhanced magnetic resonance angiography (DCE-MRA) image (B) reveals occlusion of the M1 segment of the right MCA (arrow). The conventional MRA collateral map derived from DCE-MRA (C–G) and deep learning (DL)-driven MRA collateral map (H–L) demonstrate that hypoperfused area exceeds 50% of the right MCA territory in the capillary phase (circles in D and I) compared to the collateral perfusion of the left MCA territory. Lesions with hypoperfused area in the capillary phase decreasing by less than 50% in the early venous phase (circles in E and J) are categorized as collateral perfusion score 2. The baseline DWI lesion corresponds with the hypoperfused lesion in the early venous phase of the collateral maps (circles in E and J). The collateral perfusion information provided by the two collateral maps was consistent.

We compared the time taken for collateral perfusion grading from the two collateral maps in each rater by using the Wilcoxon signed-rank test, and the sum of scores for the 6 regions of the MCA territory that were evaluated for image quality was compared by using the paired t test. The correlation between the time taken for collateral perfusion grading and image quality was analyzed by using Spearman's correlation analysis. Statistical analysis was performed by using SAS (version 9.4; Institute Inc.).

Results

The performance of 3D-MROD-Net for generating the DL-driven MRA collateral map on the test dataset of 129 nonischemic controls and 145 ischemic patients achieved ≥ 0.908 R-squared, ≥ 0.882 , tanimoto measure, ≥ 0.887 structural similarity index measure, and ≤ 0.568 mean absolute error values ($\times 10^{-1}$) on average for all five phases. 296 patients with acute ischemic stroke were selected from the DASAN to evaluate the conventional and DL-driven MRA collateral maps. For these patients, the mean age was 72 ± 13 years (range = 33–98 years), 56.1% were men (166 men and 130 women), the median baseline NIHSS score was 10 (IQR: 5–15), the median onset-to-door time was 99 min (IQR: 34–310), and the median onset-to-MRI time was 68 min (IQR: 55–92). The demographic findings of the patients with different CPSs are presented in Table 2. The presence of atrial fibrillation, a higher NIHSS score, and a larger baseline lesion volume were associated with a worse collateral perfusion grade ($P < 0.001$).

Conventional and DL-driven MRA collateral maps were generated for all patients. The interrater agreements between the two raters for collateral perfusion grading in both conventional and DL-driven MRA collateral maps were almost perfect ($\kappa = 0.93$, 95% CI: 0.91–0.96 and $\kappa = 0.94$, 95% CI: 0.92–0.96, respectively). Similarly,

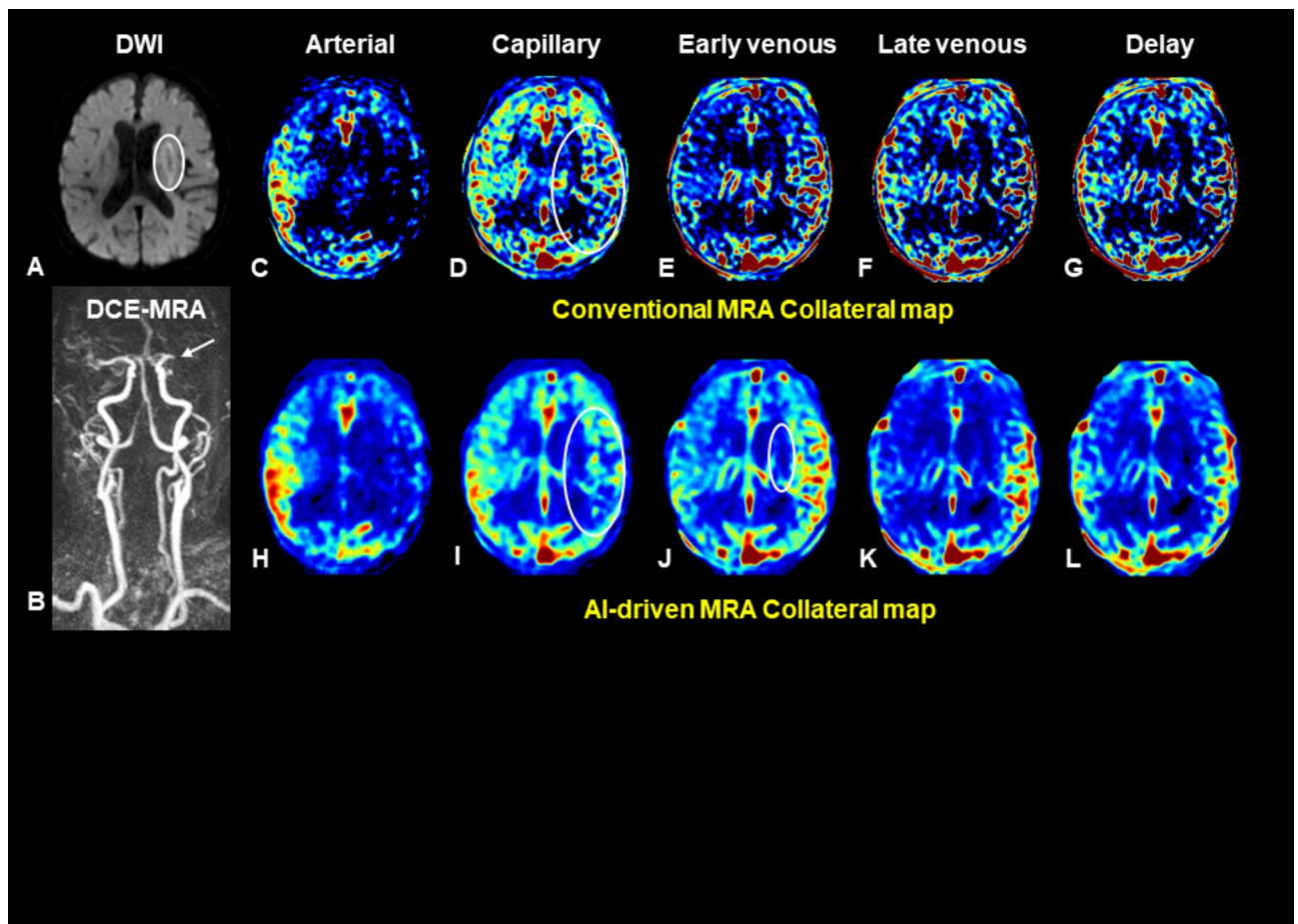


Fig. 4. Images of an elderly patient at admission. The diffusion-weighted image (DWI) (A) shows an acute infarction in the left middle cerebral artery (MCA) territory (circle). Dynamic contrast-enhanced magnetic resonance angiography (DCE-MRA) image (B) reveals occlusion of the M1 segment of the left MCA (arrow). The conventional MRA collateral map derived from DCE-MRA (C–G) and deep learning (DL)-driven MRA collateral map (H–L) demonstrate that hypoperfused area exceeds 50% of the left MCA territory in the capillary phase (circles in D and I) compared to the collateral perfusion of the right MCA territory. However, due to motion artifacts, signal intensity degradation prevents the conventional MRA collateral map from assessing the collateral perfusion state from the early venous phase onward. In contrast, the DL-driven MRA collateral map indicates hypoperfused area in the capillary phase with the area reduced to less than 50% of the left MCA territory in the early venous phase (circle in J), which corresponds to a collateral perfusion score of 2. The baseline DWI lesion corresponds with the hypoperfused lesion in the early venous phase of the collateral maps (circle in J). The DL-driven MRA collateral map compensates for severe artifacts, possibly due to the smoothing effect, in the conventional MRA collateral map, thus enabling interpretation.

the inter-method agreements of the two raters for collateral perfusion grading in both conventional and DL-driven MRA collateral maps were almost perfect ($\kappa=0.96$, 95% CI: 0.94–0.98 for rater 1 and $\kappa=0.92$, 95% CI: 0.90–0.95 for rater 2). The inter-method agreement for CPSs, as determined by the consensus of two raters, was also almost perfect ($\kappa=0.96$, 95% CI: 0.95–0.98) (Fig. 3). According to the conventional and DL-driven MRA collateral maps, CPS 5 was obtained for 22 (7.4%) and 26 patients (8.8%), respectively; CPS 4 was obtained for 36 (12.2%) and 38 patients (12.8%), respectively; CPS 3 was obtained for 58 (19.6%) and 60 patients (20.3%), respectively; CPS 2 was obtained for 80 (27.0%) and 79 patients (26.7%), respectively; CPS 1 was obtained for 44 (14.9%) and 42 patients (14.2%), respectively; and CPS 0 was obtained for 51 (17.2%) and 51 patients (17.2%), respectively. In 5 patients (1.7%), CPSs could not be assessed due to image quality degradation caused by motion artifacts in only the conventional MRA collateral maps (Fig. 4). There was a tendency for the CPSs measured on the DL-driven MRA collateral maps to be greater than those measured on the conventional MRA collateral maps (Figs. 5, 6).

For rater 1, the median time that was taken for collateral perfusion grading was 15.7 s (IQR: 9.1–24.6 s) on conventional MRA collateral maps and 12.3 s (IQR: 7.6–18.9 s) on DL-driven MRA collateral maps. For rater 2, the corresponding times were 24.0 s (IQR: 17.0–30.0 s) and 21.2 s (IQR: 15.4–28.0 s), respectively. Both raters spent significantly less time performing collateral perfusion grading on DL-driven MRA collateral maps than on conventional MRA collateral maps ($P<0.001$ for rater 1 and $P=0.003$ for rater 2). For Rater 1, the average sum

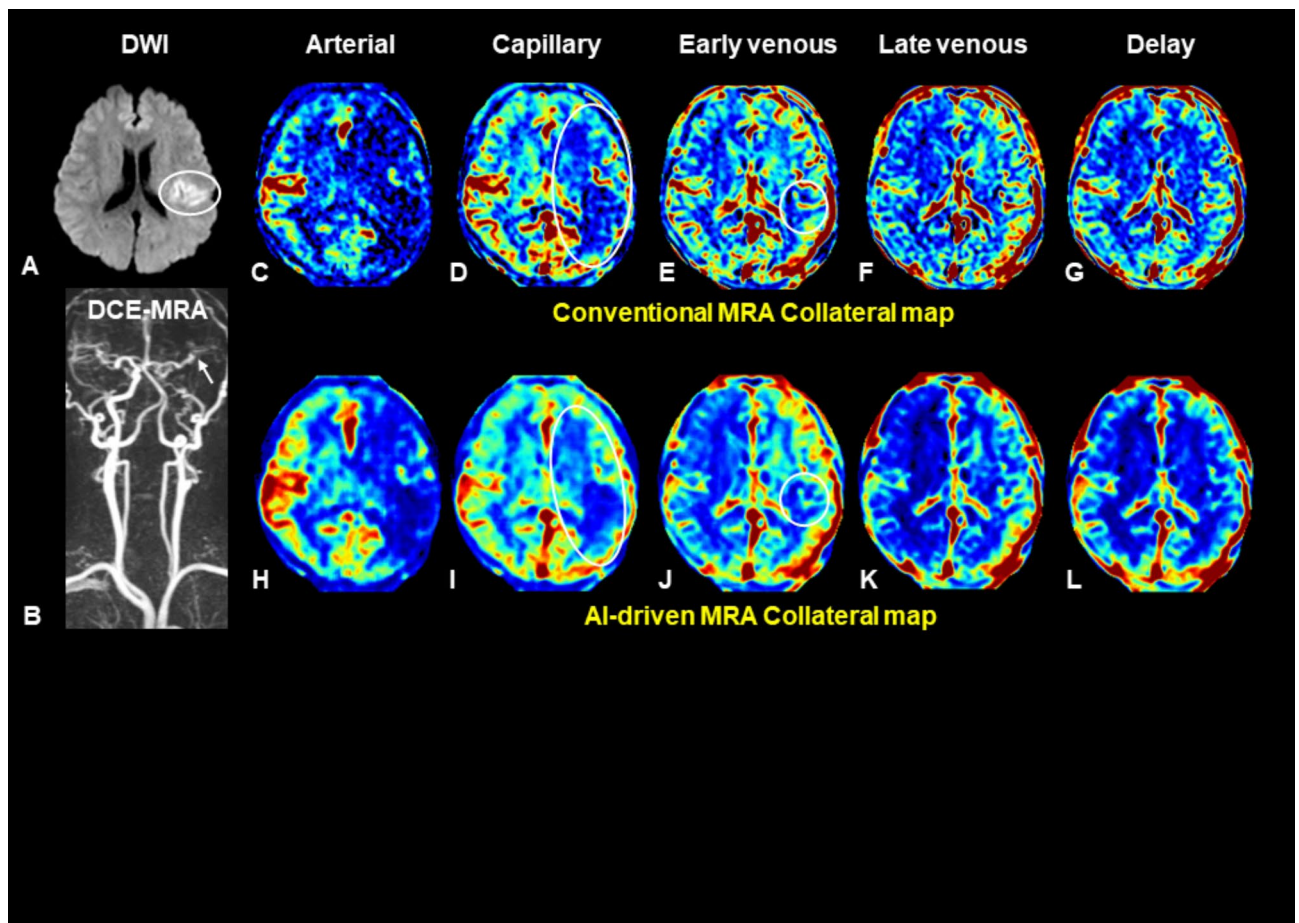


Fig. 5. Images of an elderly patient at admission. The diffusion-weighted image (DWI) (A) shows an acute infarction in the left middle cerebral artery (MCA) territory (circle). Dynamic contrast-enhanced magnetic resonance angiography (DCE-MRA) image (B) reveals occlusion of the M2 segment of the left MCA (arrow). The conventional MRA collateral map derived from DCE-MRA (C–G) and deep learning (DL)-driven MRA collateral map (H–L) demonstrate that hypoperfused area exceeds 50% of the left MCA territory in the capillary phase (circles in D and I) compared to the collateral perfusion of the right MCA territory. Lesions with hypoperfused area in the capillary phase decreasing by less than 50% in the early venous phase (circles in F and J) are categorized as collateral perfusion score 2. The baseline DWI lesion corresponds with the hypoperfused lesion in the early venous phase of the collateral maps (circles in E and J). However, due to the brightness and smoothing of the images, the hypoperfused area in the capillary phase of the DL-driven MRA collateral map may not be as distinct as that in the conventional MRA collateral map, thus leading to potential underestimation of regions with less than 50% hypoperfused area. Additionally, small hypoperfused areas remaining in the ischemic territory due to contrast washout in the opposite normal MCA territory may be overlooked, thus potentially resulting in a more favorable evaluation of collateral perfusion status in the DL-driven collateral map.

of the qualitative image quality scores of the conventional and DL-driven MRA collateral maps were 7.0 ± 2.3 (SD) and 7.7 ± 1.2 , respectively. For rater 2, the average sum values were 7.2 ± 2.1 and 7.5 ± 1.8 , respectively. The image quality that was assessed on DL-driven MRA collateral maps was significantly better than that assessed on conventional MRA collateral maps for both raters ($P < 0.001$ for rater 1 and $P = 0.002$ for rater 2). The Spearman's correlation coefficients between the time taken for collateral perfusion grading and the image quality scores of the conventional MRA collateral maps were -0.408 for rater 1 and -0.297 for rater 2 ($P < 0.001$ for both raters) and for the DL-driven MRA collateral maps, they were -0.254 ($P < 0.001$) for rater 1 and -0.143 ($P = 0.014$) for rater 2. There was a significant negative correlation between CPSs and image quality scores in both conventional and DL-driven MRA collateral maps.

Discussion

Our study showed that 3D-MROD-Net was able to generate MRA collateral maps in an accurate and robust manner and demonstrated almost perfect agreement with the conventional and DL-driven MRA collateral maps for collateral perfusion grading ($\kappa = 0.96$, 95% CI: 0.95–0.98) in patients with acute anterior circulation ischemic stroke according to both experienced and inexperienced raters (Fig. 3). In the DL-driven MRA collateral map,

Collateral perfusion score (CPS)	Description of collateral perfusion status
CPS 5 (Excellent)	No or small* hypoperfused area† in the ischemic MCA territory regardless of the collateral perfusion status in the arterial phase
CPS 4 (Good)	Hypoperfused area ≤ ½ of the ischemic MCA territory in the capillary phase, with no or small hypoperfused area in the early venous phase
CPS 3 (Intermediate to good)	(1) Hypoperfused area ≤ ½ of the ischemic MCA territory in the capillary and early venous phases (2) Hypoperfused area > ½ of the ischemic MCA territory in the capillary phase, with no or small hypoperfused area in the early venous phase
CPS 2 (Intermediate to poor)	Hypoperfused area > ½ of the ischemic MCA territory in the capillary phase with ≤ ½ of the ischemic MCA territory in the early venous phase
CPS 1 (Poor)	Hypoperfused area > ½ of the ischemic MCA territory in the early venous phase, with ≤ ½ of the ischemic MCA territory in the late venous phase
CPS 0 (Very poor)	Hypoperfused area > ½ of the ischemic MCA territory until the late venous phase

Table 1. Collateral perfusion grading system for analysis of the collateral map. *MCA* middle cerebral artery. * “Small” indicates an area smaller than 1 out of 8 MCA regions, which are divided as follows: the insula, subcortical structures (basal ganglia and internal capsule), and M1-M6 regions of the Alberta Stroke Programme Early CT Scores (ASPECTS). In visually undetermined, borderline cases with a hypoperfused area of approximately one-half of the MCA territory, the collateral perfusion score was determined by counting the number of regions with a hypoperfused area. For example, a hypoperfused area greater than one-half of the MCA territory means that the hypoperfused area involves > 4 of the 8 regions in the MCA territory.†In the capillary phase, hypoperfused area in the ischemic MCA territory is evaluated in comparison to the perfusion of the contralateral MCA territory. In the early venous, late venous and delay phases, the region that consistently demonstrates hypoperfused area observed in the capillary phase is regarded as a hypoperfused area of the ischemic MCA territory.

Characteristics	Collateral perfusion grade based on the DL-driven MRA collateral map						P value
	CPS 0	CPS 1	CPS 2	CPS 3	CPS 4	CPS 5	
No. of patients	51	42	79	60	38	26	
Men, n (%)	25 (49.0)	23 (54.8)	43 (54.4)	37 (61.7)	23 (60.5)	15 (57.7)	0.815
Age (years)*	74 ± 11	73 ± 12	71 ± 14	69 ± 13	72 ± 14	69 ± 11	0.373
Glucose at admission (mg/dl)†	124 (110–153)	123 (111–162)	126 (107–161)	128 (110–164)	133 (117–165)	132 (110–187)	0.940
Systolic blood pressure at admission (mmHg)*	149.1 ± 29.2	152.9 ± 29.7	150.6 ± 22.4	150.9 ± 27.2	148.8 ± 30.3	164.3 ± 32.7	0.259
Diastolic blood pressure at admission (mmHg)*	82.6 ± 18.4	87.5 ± 16.7	86.0 ± 14.8	85.5 ± 18.2	80.8 ± 14.3	89.3 ± 18.6	0.275
Risk factors, n (%)							
Hypertension	33 (64.7)	29 (69.0)	39 (49.4)	33 (55.0)	24 (63.2)	15 (57.7)	0.297
Diabetes	14 (27.5)	8 (19.0)	23 (29.1)	19 (31.7)	7 (18.4)	11 (42.3)	0.258
Hyperlipidemia	8 (15.7)	7 (16.7)	15 (19.0)	10 (16.7)	6 (15.8)	7 (26.9)	0.864
Atrial fibrillation	33 (64.7)	23 (54.8)	38 (48.1)	21 (35.0)	10 (26.3)	6 (23.1)	<0.001
Current smoker	3 (5.9)	6 (14.3)	16 (20.3)	9 (15.0)	5 (13.2)	5 (19.2)	0.352
Daily alcohol consumption	2 (3.9)	4 (9.5)	2 (2.5)	2 (3.3)	2 (5.3)	1 (3.8)	0.623
Previous TIA	1 (2.0)	1 (2.4)	0 (0.0)	0 (0.0)	1 (2.6)	1 (3.8)	0.213
Previous stroke	7 (13.7)	7 (16.7)	14 (17.7)	6 (10.0)	6 (15.8)	4 (15.4)	0.873
Previous ischemic heart disease	7 (13.7)	6 (14.3)	13 (16.5)	8 (13.3)	6 (15.8)	1 (3.8)	0.735
Peripheral artery disease	1 (2.0)	0 (0.0)	1 (1.3)	0 (0.0)	1 (2.6)	0 (0.0)	0.735
Baseline NIHSS score†	16 (12–20)	15 (11–19)	11 (7–15)	7 (4–12)	6 (3–9)	3 (1–6)	<0.001
Baseline DWI lesion volume (ml)†	135 (73–217)	34 (17–92)	17 (8–36)	7 (4–18)	5 (2–15)	4 (1–8)	<0.001

Table 2. Patient Characteristics (n = 296) According to the Collateral Perfusion Grade Based on the Deep Learning-driven Magnetic Resonance Angiography Collateral Map (DL-driven MRA collateral map). The mean overall patient age was 72 years ± 13 (standard deviation) (166 men and 130 women). Unless otherwise noted, the data are the number of patients, with percentages in parentheses. *CPS* collateral perfusion score, *DWI* diffusion-weighted imaging, *NIHSS* National Institutes of Health Stroke Scale. *Data are means ± standard deviations. †Data are presented as medians, with interquartile ranges in parentheses.

the time taken for collateral perfusion grading was shorter than that for collateral perfusion grading on the conventional MRA collateral map, and the image quality of the DL-driven MRA collateral map was significantly better than that of the conventional MRA collateral map. There was a negative correlation between the time taken for collateral perfusion grading and the image quality of the conventional and DL-driven MRA collateral maps. The postprocessing times that were required to generate the conventional and DL-driven MRA collateral maps were approximately 5 min and 32 s, respectively.

In our study, the presence of atrial fibrillation, a higher NIHSS score, and a larger baseline lesion volume were associated with a worse collateral perfusion grade. This finding is consistent with previous studies^{9,24}.

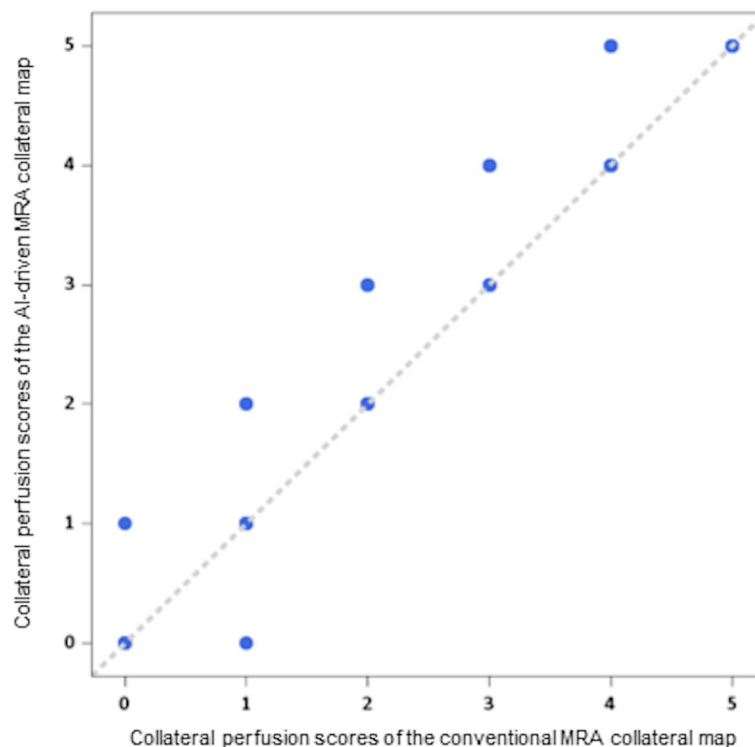


Fig. 6. Scatterplot of the agreement of the collateral perfusion scores between the conventional magnetic resonance angiography (MRA) collateral map and the deep learning (DL)-driven MRA collateral map. The inter-method agreement for collateral perfusion scores was also almost perfect (weighted kappa = 0.96, 95% confidential interval 0.95–0.98). There was a tendency for collateral perfusion scores measured on the DL-driven MRA collateral maps to be greater than those measured on the conventional MRA collateral maps.

acute ischemic stroke due to large vessel steno-occlusion is a condition that necessitates urgent treatment decisions based on imaging information, such as causative arteries, core, penumbra, and collateral perfusion status²⁵. Previous studies and commentary have demonstrated that the MRA collateral map can serve as a promising option for imaging^{7–9,26}. DCE-MRA is originally a vascular imaging technique that suppresses brain signal intensity while enhancing vessel signal intensity, particularly in conditions of acute ischemic stroke where motion artifacts are common, brain parenchymal analysis may be limited (Fig. 4). Deep learning has demonstrated its utility in various aspects of medical imaging, including data acquisition and reconstruction, imaging enhancement and correction, and interpretation of the results^{11–14}. Le et al. reported that 3D-MROD-Net showed superior performance in generating the MRP collateral map compared to the deep regression neural network, U-Net-based models and three depth estimation models; however, the MRP collateral map was unable to provide vascular information. Furthermore, they enhanced its performance by incorporating ordinal regression learning weights on important phases of the collateral map¹⁶. We successfully generated DL-driven MRA collateral maps by using 3D-MROD-Net.

The collateral perfusion estimation of the DL-driven MRA collateral map correlates well with that of the conventional MRA collateral map. This study demonstrated the clinical feasibility of DL-driven MRA collateral maps compared to conventional MRA collateral maps. The use of deep learning technology reduced the collateral map generation time by nearly tenfold. Although the generation time of conventional MRA collateral maps, which is approximately 5 min, may be acceptable, the reduction to seconds in generation time is significant in urgent conditions such as acute ischemic stroke.

Several prior works have developed and evaluated perfusion-based collateral maps^{8,9,10}. 3D-MROD-Net was originally developed for generating the MRP collateral maps. Comparing the MRA and MRP collateral maps would be highly valuable, as it could highlight their differences and respective clinical implications, which we leave for the future study. It is noteworthy that generating MRP collateral map requires additional vascular imaging to assess vascular status, which increases the amount of contrast agent used and prolongs the imaging acquisition time. With the MRA collateral maps, however, no additional imaging is needed.

MR-based imaging is prone to various artifacts, including motion artifacts, which can compromise the quality of imaging and diagnostic accuracy. In our observations, for some cases, the DL model provided better collateral maps compared to the conventional method. The improvement in image quality renders previously uninterpretable collateral maps interpretable, thus enabling collateral perfusion estimation. Although it makes image interpretation easy and rapid for some cases, the exact reasons behind these improvements remain unclear and warrant further investigation. In Fig. 4, the DL-driven collateral map was shown to be less vulnerable to motion artifacts in MRA. However, this does not imply the motion artifact capability of 3D-MROD-Net. This

may be due to the smoothing effect of the DL-driven collateral map. The specific characteristics of the DL-driven collateral map and their effects on the final interpretation need to be further investigated. Moreover, there was a drawback of the DL-driven collateral maps. As shown in Fig. 5, the images become smoother and brighter overall, thus leading to the exclusion of areas with less severe hypoperfusion from abnormal lesions and potentially resulting in more favorable collateral perfusion grade assessments, especially for inexperienced readers. The development of analysis techniques for automated collateral perfusion grading is expected to help reduce interrater differences resulting from differences in experience.

There were limitations to our study. First, all of the datasets that were used for training, testing in generating the DL-driven MRA collateral map, and clinical validation were obtained solely from the same MR scanners of two university hospitals. To further strengthen our findings, external validation with different hospital datasets is necessary. Second, this study was conducted based upon MR-based imaging. In the evaluation of patients with acute ischemic stroke, MR-based imaging work-up is considered more accurate. However, CT-based imaging work-up is often preferred due to its rapidity and easy accessibility. Recently, Yi. et al. introduced a collateral map derived from CT perfusion (CT collateral map), which is expected to serve a role similar to that of the MRA collateral map¹⁰. The collateral map not only allows for collateral perfusion assessment but also enables estimation of the baseline lesion (Figs. 3, 4, 5) and final infarct extent. Therefore, a CT-collateral map will help in overcoming the limitation of CT work-up in assessing baseline lesion extent. Clinical validation of CT collateral maps, including DL-driven CT collateral maps, is anticipated to enhance the value of collateral maps in acute ischemic stroke. Third, the same readers evaluated both the conventional and DL-driven MRA collateral maps. This raises the issues that the readers may have recognized the source of the collateral maps, potentially introducing reader bias, which could have influenced the overall evaluation of the collateral maps.

In conclusion, the clinical feasibility of the DL-driven MRA collateral map is demonstrated by its almost perfect agreement with conventional MRA collateral maps in collateral perfusion grading among patients with acute anterior circulation ischemic stroke. The DL-driven MRA collateral map offers the benefits of decreased generation and interpretation time, along with enhanced image quality of the MRA collateral map.

Data availability

The datasets generated and/or analysed during the current study are not publicly available due to IRB restriction but are available from the corresponding author on reasonable request.

Received: 2 June 2024; Accepted: 6 January 2025

Published online: 17 January 2025

References

1. Liebeskind D. S. Collaterals in acute stroke: beyond the clot. *Neuroimaging Clin. N. Am.* **15**, 553–573. <https://doi.org/10.1016/j.nic.2005.08.012> (2005). x.
2. Shuaib, A., Butcher, K., Mohammad, A. A., Saqqur, M. & Liebeskind, D. S. Collateral blood vessels in acute ischaemic stroke: a potential therapeutic target. *Lancet Neurol.* **10**, 909–921. [https://doi.org/10.1016/S1474-4422\(11\)70195-8](https://doi.org/10.1016/S1474-4422(11)70195-8) (2011).
3. Bang, O. Y. et al. Impact of collateral flow on tissue fate in acute ischaemic stroke. *J. Neurol. Neurosurg. Psychiatry* **79**, 625–629. <https://doi.org/10.1136/jnnp.2007.132100> (2008).
4. Liebeskind, D. S. et al. Collaterals at angiography and outcomes in the interventional management of stroke (IMS) III trial. *Stroke* **45**, 759–764. <https://doi.org/10.1161/STROKEAHA.113.004072> (2014).
5. Son, J. P. et al. Impact of slow blood filling via collaterals on infarct growth: comparison of mismatch and collateral status. *J. Stroke* **19**, 88–96. <https://doi.org/10.5853/jos.2016.00955> (2017).
6. Jiang, B. et al. Factors influencing infarct growth including collateral status assessed using computed tomography in acute stroke patients with large artery occlusion. *Int. J. Stroke* **14**, 603–612. <https://doi.org/10.1177/1747493019851278> (2019).
7. Jeon, Y. S. et al. Impact of collateral circulation on futile endovascular thrombectomy in acute anterior circulation ischemic stroke. *J. Korean Neurosurg. Soc.* **67**, 31–41. <https://doi.org/10.3340/jkns.2023.0139> (2024).
8. Roh, H. G. et al. A novel collateral imaging method derived from time-resolved dynamic contrast-enhanced MR angiography in acute ischemic stroke: a pilot study. *AJNR Am. J. Neuroradiol.* **40**, 946–953. <https://doi.org/10.3174/ajnr.A6068> (2019).
9. Kim, H. J. et al. Multiphase MR angiography collateral map: functional outcome after acute anterior circulation ischemic stroke. *Radiology* **295**, 192–201. <https://doi.org/10.1148/radiol.2020191712> (2020).
10. Yi, J. S. et al. The collateral map: prediction of lesion growth and penumbra after acute anterior circulation ischemic stroke. *Eur. Radiol.* **34**, 1411–1421. <https://doi.org/10.1007/s00330-023-10084-6> (2024).
11. Lee, J. G. et al. Deep learning in medical imaging: General overview. *Korean J. Radiol.* **18**, 570–584. <https://doi.org/10.3348/kjr.2017.18.4.570> (2017).
12. Cui, L. et al. Deep learning in ischemic stroke imaging analysis: a comprehensive review. *Biomed. Res. Int.* **2022** (2456550). <https://doi.org/10.1155/2022/2456550> (2022).
13. Aggarwal, R. et al. Diagnostic accuracy of deep learning in medical imaging: a systematic review and meta-analysis. *NPJ Digit. Med.* **4**, 65. <https://doi.org/10.1038/s41746-021-00438-z> (2021).
14. Chen, Z. et al. Deep learning for image enhancement and correction in magnetic resonance imaging-state-of-the-art and challenges. *J. Digit. Imaging* **36**, 204–230. <https://doi.org/10.1007/s10278-022-00721-9> (2023).
15. To, M. N. N., Kim, H. J., Roh, H. G., Cho, Y. S. & Kwak, J. T. Deep regression neural networks for collateral imaging from dynamic susceptibility contrast-enhanced magnetic resonance perfusion in acute ischemic stroke. *Int. J. Comput. Assist. Radiol. Surg.* **15**, 151–162. <https://doi.org/10.1007/s11548-019-02060-7> (2020).
16. Le, H. L., Roh, H. G., Kim, H. J. & Kwak, J. T. A 3D multi-task regression and Ordinal regression deep neural network for collateral imaging from dynamic susceptibility contrast-enhanced MR perfusion in acute ischemic stroke. *Comput. Methods Programs Biomed.* **225**, 107071. <https://doi.org/10.1016/j.cmpb.2022.107071> (2022).
17. Lee, T. J. et al. Collateral and permeability imaging derived from dynamic contrast material-enhanced MR angiography in prediction of PH 2 hemorrhagic transformation after acute ischemic stroke: a pilot study. *Neuroradiology* **63**, 1471–1479. <https://doi.org/10.1007/s00234-021-02655-5> (2021).
18. Lee, H. J. et al. Collateral estimation by susceptibility-weighted imaging and prediction of functional outcomes after acute anterior circulation ischemic stroke. *Sci. Rep.* **11**, 21370. <https://doi.org/10.1038/s41598-021-00775-9> (2021).
19. Lee, T. J. et al. Prognostic value of collateral perfusion estimation by arterial spin labeling for acute anterior circulation ischemic stroke. *Neuroradiology* **65**, 1695–1705. <https://doi.org/10.1007/s00234-023-03233-7> (2023).

20. Bak, S. H., Roh, H. G., Moon, W. J., Choi, J. W. & An, H. S. Appropriate minimal dose of gadobutrol for 3D time-resolved MRA of the supra-aortic arteries: comparison with conventional single-phase high-resolution 3D contrast-enhanced MRA. *AJNR Am. J. Neuroradiol.* **38**, 1383–1390. <https://doi.org/10.3174/ajnr.A5176> (2017).
21. Ryu, W. S. et al. Acute infarct segmentation on diffusion-weighted imaging using deep learning algorithm and RAPID MRI. *J. Stroke* **25**, 425–429. <https://doi.org/10.5853/jos.2023.02145> (2023).
22. Barber, P. A., Demchuk, A. M., Zhang, J. & Buchan, A. M. Validity and reliability of a quantitative computed tomography score in predicting outcome of hyperacute stroke before thrombolytic therapy. ASPECTS Study Group. Alberta Stroke Programme early CT score. *Lancet* **355**, 1670–1674 (2000).
23. Landis, J. R. & Koch, G. G. The measurement of observer agreement for categorical data. *Biometrics* **33**, 159–174 (1977).
24. Kim, S. J. et al. A novel magnetic resonance imaging approach to collateral flow imaging in ischemic stroke. *Ann. Neurol.* **76**, 356–369. <https://doi.org/10.1002/ana.24211> (2014).
25. Kim, H. J. & Roh, H. G. Imaging in acute anterior circulation ischemic stroke: current and future. *Neurointervention* **17**, 2–17. <https://doi.org/10.5469/neuroint.2021.00465> (2022).
26. Lu, S. S. & Multiphase MR angiography collateral map in brain stroke: may we shift the time from an absolute to the relative for therapy decisions? *Eur. Radiol.* **34**, 1409–1410. <https://doi.org/10.1007/s00330-023-10275-1> (2024).

Acknowledgements

The authors are grateful to Myeong Hee Kim and Dawoon Kim, who helped them maintain the DASAN registry as research assistants.

Author contributions

1. Conceptualization: Hyun Jeong Kim, Jin Tae Kwak, Ye Jin Jeon, Hong Gee Roh. 2. Data curation: Ye Jin Jeon, Hong Gee Roh, Hee Jong Ki, Jeong Jin Park, Taek-Jun Lee, Ji Sung Lee, Jin Tae Kwak, Hyun Jeong Kim. 3. Formal analysis: Ye Jin Jeon, Hong Gee Roh, Sumin Jung, Hyun Yang, Hee Jong Ki, Jeong Jin Park, Taek-Jun Lee, Na Il Shin, Ji Sung Lee, Jin Tae Kwak, Hyun Jeong Kim. 4. Funding acquisition: Hong Gee Roh, Hee Jong Ki, Jin Tae Kwak, Hyun Jeong Kim. 5. Investigation: Ye Jin Jeon, Hong Gee Roh, Sumin Jung, Hyun Yang, Hee Jong Ki, Jeong Jin Park, Taek-Jun Lee, Na Il Shin, Ji Sung Lee, Jin Tae Kwak, Hyun Jeong Kim. 6. Methodology: Ye Jin Jeon, Hong Gee Roh, Sumin Jung, Hyun Yang, Hee Jong Ki, Jeong Jin Park, Taek-Jun Lee, Na Il Shin, Ji Sung Lee, Jin Tae Kwak, Hyun Jeong Kim. 7. Project administration: Hong Gee Roh, Hee Jong Ki, Jin Tae Kwak, Hyun Jeong Kim. 8. Resources: Ye Jin Jeon, Hong Gee Roh, Sumin Jung, Hyun Yang, Hee Jong Ki, Jeong Jin Park, Taek-Jun Lee, Na Il Shin, Ji Sung Lee, Jin Tae Kwak, Hyun Jeong Kim. 9. Software: Ye Jin Jeon, Hong Gee Roh, Sumin Jung, Hyun Yang, Jin Tae Kwak, Hyun Jeong Kim. 10. Supervision: Jin Tae Kwak, Hyun Jeong Kim. 11. Validation: Ye Jin Jeon, Hong Gee Roh, Sumin Jung, Hyun Yang, Hee Jong Ki, Jeong Jin Park, Taek-Jun Lee, Na Il Shin, Ji Sung Lee, Jin Tae Kwak, Hyun Jeong Kim. 12. Visualization: Ye Jin Jeon, Hong Gee Roh, Sumin Jung, Hyun Yang, Jin Tae Kwak, Hyun Jeong Kim. 13. Writing—original draft: Ye Jin Jeon, Hong Gee Roh, Sumin Jung, Hyun Yang, Hee Jong Ki, Jeong Jin Park, Taek-Jun Lee, Na Il Shin, Ji Sung Lee, Jin Tae Kwak, Hyun Jeong Kim. 14. Writing—review & editing: Ye Jin Jeon, Hong Gee Roh, Sumin Jung, Hyun Yang, Hee Jong Ki, Jeong Jin Park, Taek-Jun Lee, Na Il Shin, Ji Sung Lee, Jin Tae Kwak, Hyun Jeong Kim.

Funding

This study was supported by grants from the National Research Foundation of Korea (NRF) (No. RS-2023-00266130, RS-2023-00248375, and RS-2023-00252980) and Korea Institute of Startup and Entrepreneurship Development (No. 20228485) from the Korean government.

Declarations

Competing interests

Ye Jin Jeon, Sumin Jung, Hyun Yang, Hee Jong Ki, Jeong Jin Park, Take-Jun Lee, Na Il Shin, and Ji Sung Lee have no financial interests. Hong Gee Roh, Jin Tae Kwak, and Hyun Jeong Kim are founders of DeepClue Inc.

Additional information

Correspondence and requests for materials should be addressed to J.T.K. or H.J.K.

Reprints and permissions information is available at www.nature.com/reprints.

Publisher's note Springer Nature remains neutral with regard to jurisdictional claims in published maps and institutional affiliations.

Open Access This article is licensed under a Creative Commons Attribution-NonCommercial-NoDerivatives 4.0 International License, which permits any non-commercial use, sharing, distribution and reproduction in any medium or format, as long as you give appropriate credit to the original author(s) and the source, provide a link to the Creative Commons licence, and indicate if you modified the licensed material. You do not have permission under this licence to share adapted material derived from this article or parts of it. The images or other third party material in this article are included in the article's Creative Commons licence, unless indicated otherwise in a credit line to the material. If material is not included in the article's Creative Commons licence and your intended use is not permitted by statutory regulation or exceeds the permitted use, you will need to obtain permission directly from the copyright holder. To view a copy of this licence, visit <http://creativecommons.org/licenses/by-nc-nd/4.0/>.

© The Author(s) 2025